JOURNAL OF THE KOREAN ASTRONOMICAL SOCIETY
32: 91 ~ 107, 1999

OPTICAL AND NIR PHOTOMETRY OF OPEN CLUSTER NGC 7790

JUNG-DEOK LEE AND SANG-GAK LEE
Department of Astronomy , Seoul National University, Seoul 151-742, Korea
E-mail: leejd@astro.snu.ac.kr, sanggak@astrosp.snu.ac.kr
(Received Oct. 1, 1999; Accepted Oct. 12, 1999)

ABSTRACT

We present BVRI CCD photometry and near-infrared K photometry of the intermediate-aged open cluster NGC 7790. The reddening, $E(B-V) = 0.54 \pm 0.05$ and the distance modulus, $(m-M)_o = 12.45 \pm 0.10$ for the cluster were determined by zero-age-main-sequence fitting and theoretical isochrone fitting using not only $(V, B-V), (V, V-I), (V, V-R)$ but also $(V, V-K)$ color-magnitude diagrams. The reddening corresponded approximately to the average value derived from previous studies, while the distance modulus was found to be almost midway between the CCD photometric results of Romeo et al. (1989) and those of Mateo & Madore (1988). We have used four colors to distinguish members from field stars. The expected colors were calculated using the derived distance modulus, and were then were compared with the observed colors $(B-V), (V-I), (V-R)$, and $(V-K)$. Thus, a color excess $E(B-V)$ for each star was determined which could give the minimum difference between the calculated and observed colors. Single and binary members of the cluster were determined on the basis of the $E(B-V)$ distribution of stars.

Key words : clusters : open - clusters : individual (NGC 7790) - clusters : NIR photometry - clusters : membership - clusters : general

I. INTRODUCTION

Open clusters are useful tools for analyzing the large-scale properties of the disk of the Galaxy and for testing theories of stellar and galactic evolution especially with regard to the galactic disk. More than 1200 open clusters have been discovered (Lyngå 1987) but only one-third of these clusters have been studied. Nevertheless, studies of open clusters have confirmed the metallicity gradient with galactocentric distance (Janes 1979, Panagia & Tosi 1981) and have provided evidence to support the density wave theory. Recently, Piatti et al. (1995) found a radial abundance gradient, $\partial[Fe/H]/\partial R_{GC} = -0.07$ dex/kpc, as well as a steeper abundance gradient perpendicular to the Galactic plane , $\partial[Fe/H]/\partial|Z| = -0.34$ dex/kpc. The age distribution of the open clusters overlaps that of globular clusters thereby suggesting that the disk started to form before the end of the period of halo formation(Janes & Phelps 1994).

Intermediate-aged open clusters are especially valuable for the study of the evolution and photometric properties of intermediate mass stars(Sung & Bessell 1998).

If clusters contain classical Cepheids, they are of great importance because they can provide intrinsic luminosities for the calibration of the period-luminosity-color (PLC) relation(Sandage & Tammann 1969). Although Cepheids have been studied extensively since the discovery of the fundamental period-luminosity (PL) relationship, the metallicity dependence of this relation still remains uncertain. Recently, the metallicity effects on the PLC relation have been investigated by many groups but the results have been rather controversial(Sekiguchi & Fukgita 1998 ; Tanvir 1997). In a separate study employing a computed grid of atmosphere models and synthetic spectra for different metallicities, no significant effect of metallicity on the PL relationship was found in the V and K magnitudes(Alibert et al. 1999).

NGC 7790 is an intermediate-aged cluster (Mermilliod 1981) containing three Cepheids and an eclipsing binary. The cluster is of intermediate richness (Janes & Adler 1982) and is located in the galactic disk near the Perseus arm (RA=$23^h55^m.9$, Dec.=+60°56′, l = 116°.6, b = −1°.0). Although there have been many previous studies (Kraft 1958; Sandage 1958; Schmidt 1981; Pedreros, Madore, & Freedman 1984(hereafter PMF), Matthews et al. 1995), the basic properties of the cluster, the reddening and distance modulus are not yet completely settled. The distance modulus ranges from $(m-M)_o = 11.98 \pm 0.13$(Schmidt 1981) to 12.80 ± 0.15 (Sandage 1958) and the reddening varies from $E(B-V) = 0.49 \pm 0.024$ (Kraft 1958, 1981) to 0.64 ± 0.04 (PMF). The first BVRI CCD observations of NGC 7790 by Romeo et al. (1989, hereafter RBFT) gave a reduced distance modulus of $(m-M)_o = 12.65 \pm 0.15$ using the Pleiades as the ZAMS fiducial line. Independent $UBVR$ CCD photometry of NGC 7790 by Mateo & Madore (1989) resulted in a value of $(m-M) = 12.33 \pm 0.15$ by adopting almost the same reddening as RBFT and using both the Pleiades and a theoretical isochrone (Vanden Bergh & Bridges 1988) for their ZAMS fits.

These inconsistent results for the cluster may be due

Table 1. The optical observations

filter	exp. time(sec)	number of image	obs. date	seeing(arcsec)
B	30	5	98. 11. 9	3.14
V	20	5	98. 11. 9	2.46
R	5	5	98. 11. 9	2.42
I	5	7	98. 11. 9	2.20

Table 2. The NIR K observations

region	exp. time(sec)	number of image	obs. date	seeing(arcsec)
center	3	45	97. 7. 3	~ 2.5
NE	3	45	97. 7. 3	~ 2.5
NW	3	45	97. 7. 3	~ 2.5
SE	3	45	97. 7. 4	~ 2.5
SW	3	45	97. 7. 4	~ 2.5

to its relatively wide main sequence and turn-off, part of which were contaminated by field stars. So the distinction between the cluster members and field stars is especially important for this cluster. The best method of distinguishing membership is to obtain kinematic information on the stars, either radial velocities or proper motions, but in the case of NGC 7790, such measurements are not yet feasible since the cluster is too distant. Therefore, we make use of the advantage given by observations in multiple colors including the near IR band to select the cluster members. In Section II, the CCD observations and the reductions of the CCD and near IR photometry on the cluster are discussed. The reddening, distance modulus, age, and membership of the cluster are analyzed in Section III, and discussion and summary follow in Section IV.

II. OBSERVATION AND REDUCTION

(a) Observation

Optical BVRI observations were made on a non-photometric day in Nov. 1998 at BOAO (Bohyun Optical Astronomical Observatory) using a Tek 2048 × 2048 CCD camera mounted on the 1.8m telescope(f/8). The gain and the readout noise of the Tek CCD camera are 9 e^-/ADU and 10.4 e^-. The field size is 12′ × 12 ′ (0.34″/pixel) and CCD standard stars(Christian et al. 1985) were included in the same region as NGC 7790. The observation log is presented in Table 1.

The NIR K-band observations were made on non-photometric days in Jul. 1997 with the 2.1m telescope at KPNO using the IR-array IRIM(256 × 256 pixel ; 1.09 arcsec/pixel) by Lee, Carney, & Oh (1998). IRIM's gain and readout noise are 10.46 e^-/ADU and 35 e^-, respectively.

Each pixel in IRIM is essentially independent of the others. This independence means that such properties as linearity and dark current can vary from pixel to pixel, and it is necessary to calibrate these effects for optimum scientific performance. Although the real noise of the dark current is quite low($2e^-$/s), the dark current cannot be simply scaled with time. Therefore dark frames were taken repeatedly for each integration time at the beginning and end of the observation.

The field of view is 280″ × 280″. Images of the cluster were obtained for the central, NE, NW, SE, and SW regions in the dither mode covering a total field of view of about 8′ × 8′, which contains almost the entire region of the cluster. In the NIR K-band the sky level was very high, i.e., about 10,000 ADU for a 3-sec exposure. To avoid sky saturation, 45 short exposure frames were taken for five regions. Each field image-set was composed of five shifted images in order to avoid many bad pixels in IRIM.

For photometric standardization, the faint JHK standards of UKIRT(Casali & Hawarden 1992) observed during the observing run were used. The log of NIR observations is presented in Table 2.

In Fig. 1 the stars whose magnitudes were measured in the B, V, R, and I bands stars are represented by open circles and the filled circles represent those whose magnitudes were additionally measured in the K band.

(b) Reduction

The optical images were preprocessed using the IRAF/ccdred package. Since the crowding increases toward the central region of the cluster, instrumental magnitudes were obtained using PSF fitting in the IRAF/daophot package(Stetson 1987, 1990).

NIR image reduction was also done using the IRAF/ccdred package, but minor preprocessing from optical images was performed owing to the non-linearity of the IR detector. The non-linearity of the dark current was

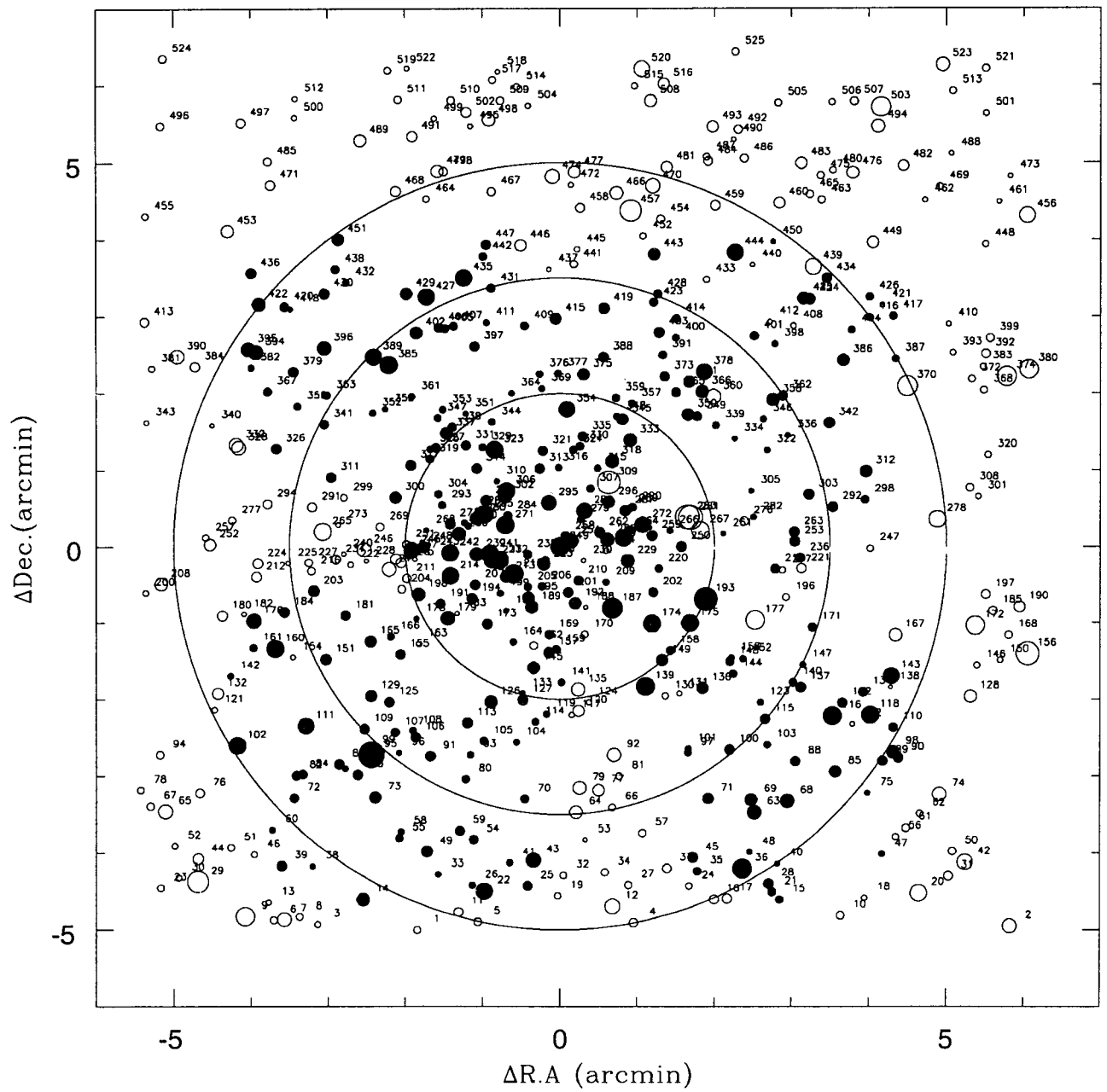

Fig. 1.— Identification map for the stars measured. The open circles represent stars with B, V, R, and I magnitudes and the filled circles are the stars with B, V, R, I, and K magnitudes. The 3 large circles denote radii r=2.0, 3.5, 5.0′ from the center of the cluster. North is up, and east is left.

corrected by subtracting the dark image with the same exposure time as the object image. The ten dark images of 3 second duration thus obtained were combined to produce a master dark frame.

The master sky images were obtained by combining five shifted sky images, and they were subtracted from the object images. Also, the median-combined sky images which were observed between the field observations were used as flat images. Every sky-subtracted cluster image was flattened using the master sky image which was obtained at the time closest to the observing time, then each set of images was shifted and median-combined for photometry.

The instrumental magnitudes were obtained using the IRAF/daophot package. For the cluster stars, the instrumental K magnitudes were obtained by using PSF photometry because of crowding in the cluster field, while for the standard stars, they were measured by aperture photometry.

(c) Magnitude Calibration

CCD standard stars in NGC 7790 in Christian et al. (1985) are used for the standardization of optical $BVRI$ magnitudes, since no other standard stars were observed separately. The ten CCD standard stars in NGC 7790 are located in the south-east region of the field in Fig. 1. The following standardization equations are used for translating to the standard system and each coefficient is shown in Table 3.

$$\begin{aligned} V - v &= a \cdot (B - V) + C_V \\ (B - V) &= b \cdot (b - v) + C_{(B-V)} \\ (V - I) &= c \cdot (v - i) + C_{(V-I)} \\ (V - R) &= d \cdot (v - r) + C_{(V-R)}, \end{aligned}$$

where the small letters represent instrumental magnitudes, the capitals standard magnitudes, and Cs with subscripts zero points. In these formulae the airmass term is omitted since we used the standard stars in the same area of the sky as the cluster.

Many authors have used the photoelectric standard stars of Sandage (1958) for calibration since these stars, which are very numerous, are widely spread over a sufficient range in color, and are quite uniformly distributed over the field of the cluster. However, these stars have only U, B, and V magnitudes.

Alcalá & Arellano Ferro(1988) performed $UBVRI$ (Kron-Cousins) photometry of a group of stars in NGC 7790 but comparison of their photoelectric photometry with that of Sandage (1958) shows the following differences: $\Delta V = -0.008$, $\Delta(U - B) = -0.042$, and $\Delta(B - V) = -0.020$.

The CCD standard stars of Christian et al. (1985) in the field of NGC 7790 are observed in the B, V, R, I bands but they are all located toward one side of the cluster and have relatively large σ values. Among these CCD standard stars, K and S stars were observed by Sandage (1958). However, their magnitudes show large discrepancies (Sandage-Christian et al.), with $\Delta V = -0.068$, 0.001 and $\Delta(B - V) = 0.020$, -0.084 for S and for K, respectively. The star 16 is included in the stars of Alcalá & Arellano Ferro(1988) and shows large differences in measured magnitudes (Alcalá & Arellano Ferro - Christian et al.), with $\Delta V = 0.150$, $\Delta(B-V) = 0.003$, $\Delta(V - I) = 0.239$, and $\Delta(V - R) = 0.241$. Nevertheless, the observations of standard stars by Christian et al. (1985) were made for the same B, V, R, and I bands as this study and they include sufficiently faint stars, so we prefer to use them for calibration of the magnitudes of stars.

Comparison of our calibrated magnitudes and colors with those of RBFT shows systematic magnitude and color differences, which are shown in Fig. 2. The systematic color differences are −0.03, 0.01, 0.07 for (B-V), (V-R), (V-I) colors; the (B-V) color differences between this study and that of RBFT show a trend in which RBFT's colors are redder for fainter stars. The slopes of the residuals, shown in the right panel of Fig. 2, are 0.0053 in V, 0.0113 in B, 0.044 in I, and 0.0100 in R. These differences may be due to the use of different standard stars. RBFT used stars from Sandage (1958) and a revised PMF for B and V, whereas Christian et al. (1985) employed R and I. We compared the transformed B, V magnitudes of this study to the magnitudes of Sandage (1958)'s photometric standard stars. In Fig. 3, no trend in magnitude or color is found, except for small systematic differences in B and V.

NIR standardization was done according to the procedure in "The faint standard stars for UKIRT" (Casali & Hawarden 1992). There is no evidence for a color term in the transformation to the standard K system(Lee, Carney, & Probst 1997). The transformation equation is

$$k - K = a \cdot X + C_K,$$

where X is the airmass. In the K band, the atmospheric extinction varied from 0.05/mag to 0.15 mag/airmass due to the humidity(Lee, Carney, & Probst 1997). These observations were carried out in the most humid period(July 1997), and the days we performed observations were not photometric with a high atmospheric extinction coefficient of about 0.18 mag/airmass, with $a = 0.1819 \pm 0.0187$, and $C_K = 4.4516 \pm 0.0229$.

The stars in the central region of the cluster field were transformed to the standard system using the above equation. The magnitudes of stars in the other fields were corrected to match those of the same stars in the region overlapping the central field.

The results of the photometry are presented in Table 4. Table 4 contains only the stars which possess all B, V, R, I, and K magnitudes(filled circles in Fig. 1).

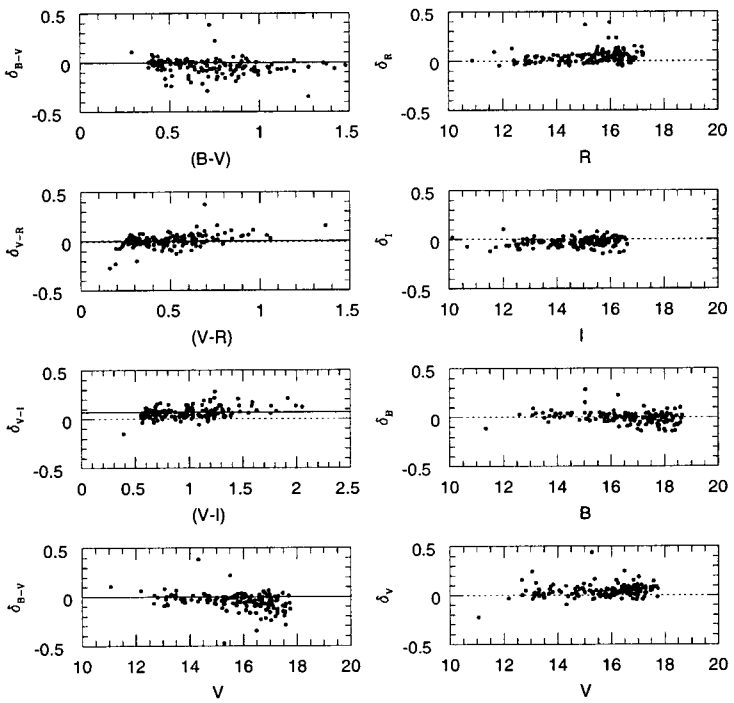

Fig. 2.— Differences between our magnitudes and those of RBFT.

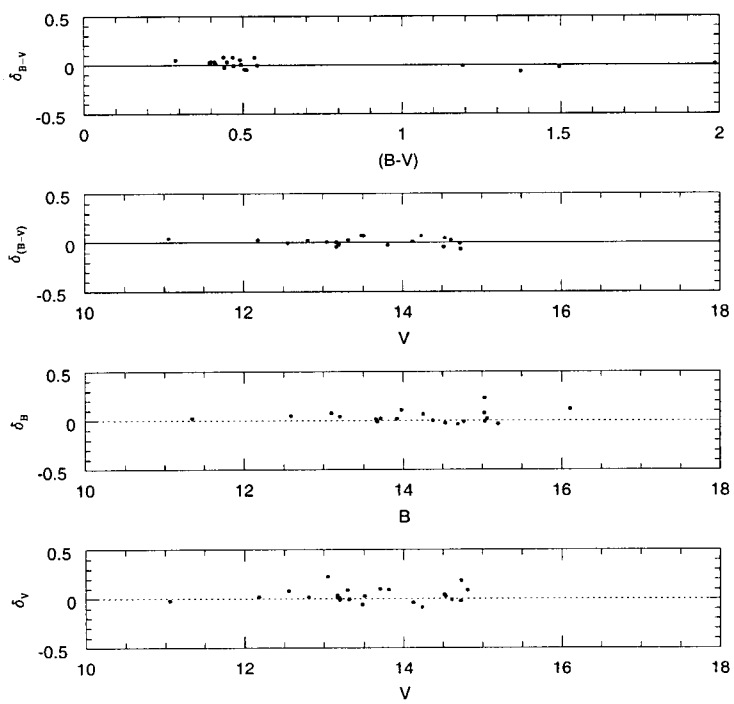

Fig. 3.— Differences between our magnitudes and those of Sandage (1958)'s standard stars.

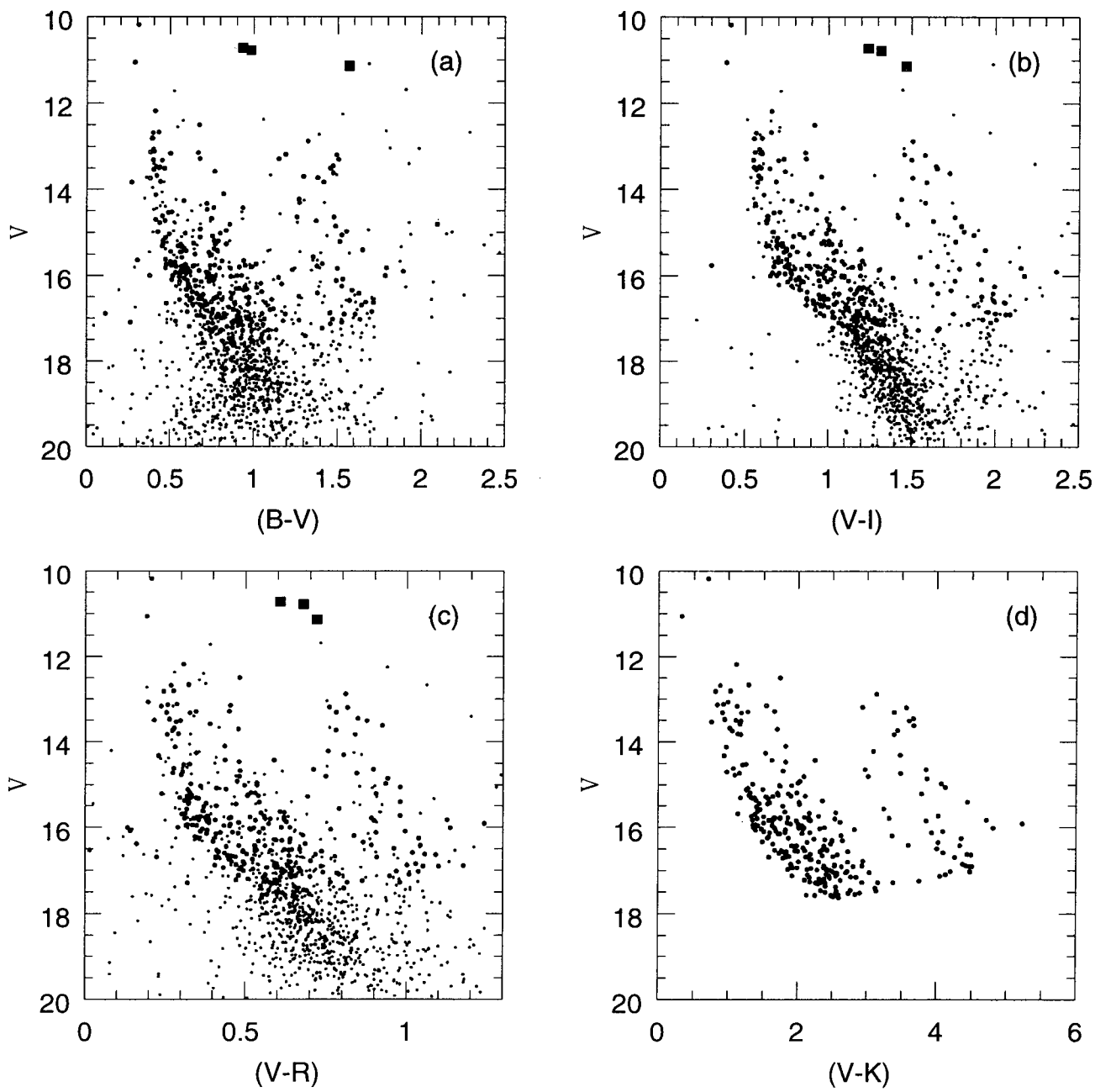

Fig. 4.— Color-Magnitude Diagram of NGC 7790 (a) (V,B-V) CMD (b)(V,V-I) CMD (c) (V,V-R) CMD (d) (V,V-K) CMD. In (a),(b), and (c), large dots indicate that the V magnitude errors are less than 0.1 mag and the color magnitude errors are less than 0.05 mag. The filled squares are Cepheids.

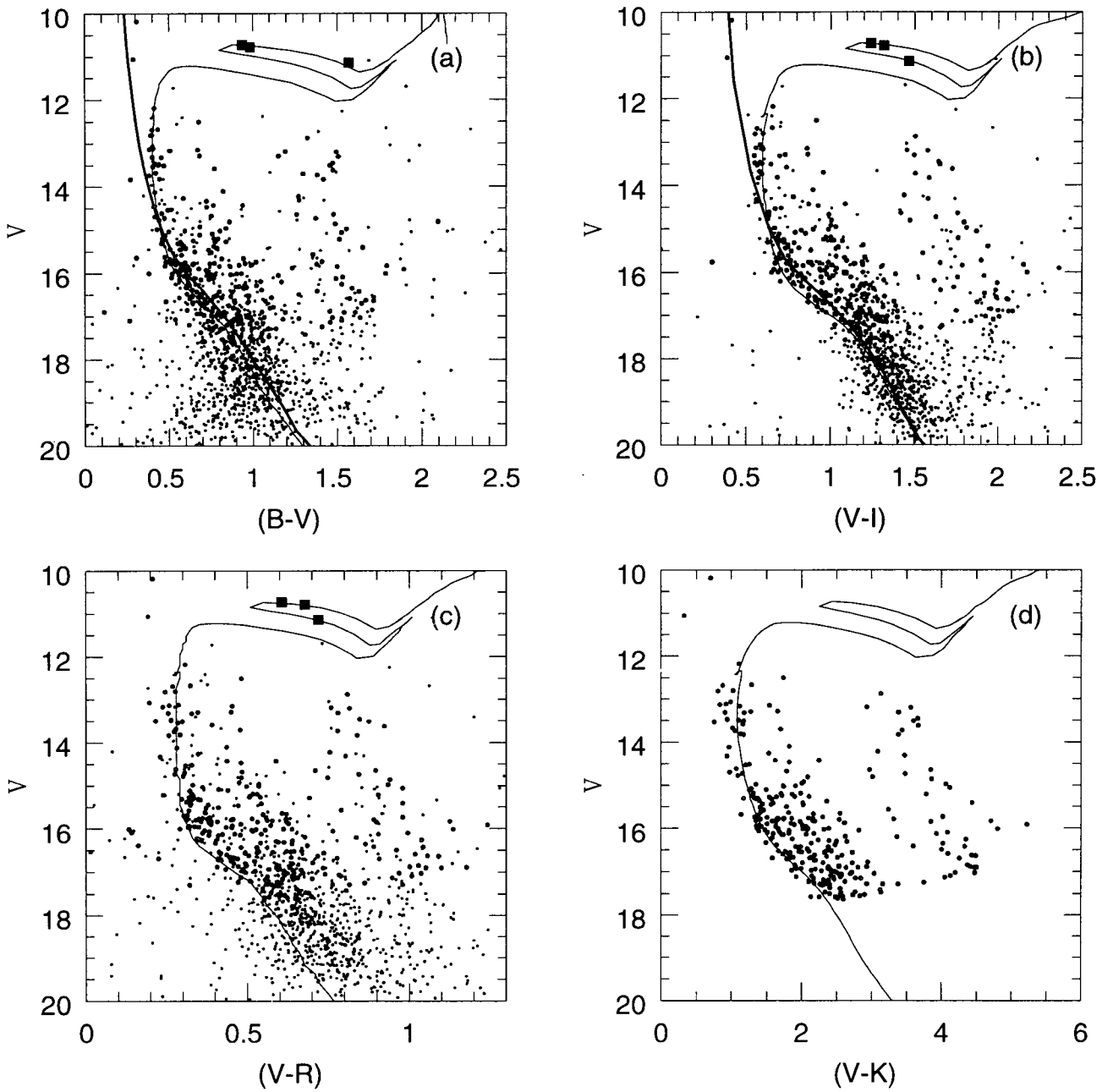

Fig. 6.— Our best fit result. The thick solid line is the ZAMS(Sung & Bessell 1999) and the thin solid line is the theoretical isochrone(Bertelli et al. 1994), log(age) = 8.1, [Fe/H]=-0.32). The filled squares denote Cepheid Variables.

Table 3. The value of the translation coefficient

coefficient	a	C_V	b	$C_{(B-V)}$	c	$C_{(V-I)}$	d	$C_{(V-R)}$
value	0.0052	−1.9117	1.1703	−0.5118	0.9388	0.0791	0.9318	0.0647
error	±0.0788	±0.0488	±0.0163	±0.0173	±0.0325	±0.0302	±0.1613	±0.0220

Table 4. The photometric results NGC 7790

ID	XC(″)	YC(″)	V	$(B-V)$	$(V-I)$	$(V-R)$	K	σ_K	Membership
14	-152.85	-276.38	14.81	0.86	1.01	0.48	12.72	0.05	
15	171.03	-276.33	16.63	1.07	1.28	0.72	14.06	0.04	
21	165.13	-270.25	16.55	0.67	1.00	0.53	14.55	0.04	
22	-58.44	-269.75	13.46	1.47	1.65	0.85	9.80	0.13	
25	-24.89	-265.67	16.15	0.69	0.85	0.41	14.43	0.21	M
26	-67.86	-265.19	17.05	1.27	1.40	0.74	14.01	0.16	
28	162.56	-263.78	15.90	0.57	0.78	0.39	14.39	0.08	M
33	-94.33	-256.72	17.28	1.09	1.66	0.98	13.90	0.16	
35	106.9	-254.22	16.56	1.11	1.33	0.74	13.84	0.03	
36	142.12	-252.26	12.50	0.68	0.92	0.48	10.76	0.03	
38	-192.07	-250.41	17.42	1.31	1.47	0.81	14.30	0.11	
39	-216.07	-250.13	15.80	0.99	1.15	0.56	13.27	0.14	
40	169.37	-248.23	17.61	0.89	1.24	0.65	15.10	0.11	M
41	-38.8	-247.55	17.16	1.02	1.34	0.64	14.31	0.22	
43	-20.38	-245.49	14.22	1.27	1.44	0.76	11.13	0.11	
45	103.43	-243.58	15.75	0.59	0.76	0.36	14.24	0.08	M
47	250.3	-240.71	17.12	0.76	1.08	0.48	15.20	0.07	M
48	147.72	-239.06	17.31	0.76	1.15	0.60	15.02	0.05	M
49	-103.1	-238.75	15.45	0.56	0.74	0.32	13.89	0.20	M
54	-66.68	-229.23	16.31	0.90	1.24	0.61	13.66	0.20	
55	-124.53	-228.23	16.69	1.64	1.88	0.91	12.43	0.18	
58	-123.28	-223.28	17.06	0.93	1.18	0.62	14.36	0.04	
59	-77.41	-222.54	16.12	1.49	1.76	0.91	12.19	0.18	
60	-223.41	-221.78	17.24	1.41	1.67	0.86	13.49	0.12	
63	151.38	-208.18	14.43	0.94	1.09	0.59	12.18	0.04	
68	177.06	-199.48	14.47	0.72	0.93	0.48	12.65	0.04	
69	148.86	-198.47	15.04	0.50	0.83	0.36	13.29	0.03	M
70	-27.11	-197.9	16.53	0.87	1.22	0.64	14.11	0.12	
71	115.31	-197.63	15.67	0.81	1.09	0.55	13.50	0.07	
72	-206.3	-197.3	16.35	1.59	1.74	0.87	12.33	0.09	
73	-143.34	-196.63	15.27	0.57	0.70	0.32	13.63	0.21	M
75	238.86	-193.26	17.53	1.00	1.27	0.60	14.97	0.06	B
80	-72.82	-182.44	16.69	0.72	0.98	0.47	14.57	0.13	M
82	-204.58	-179.59	16.22	0.61	0.71	0.34	14.64	0.13	M
83	-157.04	-179.14	15.96	0.60	0.78	0.35	14.33	0.18	M
84	-199.79	-178.75	16.32	0.96	1.14	0.54	13.83	0.08	
85	214.26	-176.53	15.19	0.77	1.01	0.52	13.21	0.04	
86	-166.68	-174.23	17.37	0.69	1.12	0.55	14.97	0.10	
87	-171.37	-170.85	15.84	0.61	0.80	0.39	13.86	0.07	M
88	183.26	-168.61	16.01	1.79	2.17	1.14	11.20	0.02	
89	250.74	-168.18	15.92	0.62	1.04	0.57	14.02	0.06	B
90	262.91	-165.86	16.01	0.93	1.20	0.64	13.62	0.07	
91	-100.34	-164.64	15.80	0.57	0.74	0.34	14.13	0.11	M
93	-69.23	-163.42	17.03	1.64	2.01	1.04	12.55	0.14	
95	-146.43	-163.39	10.18	0.31	0.42	0.21	9.48	0.08	
96	-124.81	-161.9	17.48	1.05	1.35	0.66	14.34	0.05	
97	99.56	-161.88	16.91	0.79	1.19	0.60	14.27	0.05	B
98	258.62	-161.18	14.86	1.49	1.80	0.94	11.00	0.07	
99	-147.83	-160.03	13.83	0.27	0.58	0.26	12.65	0.13	M
100	132.06	-159.44	15.88	1.23	1.31	0.63	13.27	0.06	
101	99.87	-158.85	17.07	0.54	1.33	0.78	14.52	0.08	
102	-250.52	-156.22	13.31	1.51	1.50	0.78	9.93	0.05	
103	161.48	-155.66	16.91	1.54	2.09	1.05	12.40	0.08	
104	-33.4	-153.58	17.28	1.14	1.54	0.82	14.12	0.07	
105	-58.8	-152.66	16.62	0.75	1.05	0.51	14.44	0.09	B
106	-111.87	-149.7	15.93	0.72	0.94	0.45	13.92	0.09	B
107	-127.83	-145.85	16.30	0.92	1.19	0.60	13.80	0.09	
108	-114.02	-144.49	16.87	0.91	1.18	0.47	14.34	0.09	B
109	-151.78	-143.25	16.03	0.87	1.08	0.56	13.71	0.07	
110	258.98	-142.01	16.27	0.95	1.21	0.64	14.03	0.02	
111	-197.31	-140.78	13.73	1.38	1.51	0.78	10.29	0.09	
113	-71.59	-138.41	15.77	0.77	0.30	0.52	13.67	0.06	
114	-18.87	-137.52	16.85	1.71	1.96	1.03	12.48	0.09	
115	159.68	-135.61	15.91	1.89	2.36	1.24	10.68	0.05	
116	211.86	-133.09	12.88	1.32	1.51	0.81	9.75	0.06	
118	241.2	-132.26	13.15	0.67	0.86	0.45	11.61	0.04	
119	-10.27	-131.52	17.02	1.47	1.93	0.97	12.82	0.09	
122	219.6	-122.7	16.11	0.65	0.95	0.46	14.30	0.07	
123	156.05	-122.48	17.10	0.73	1.07	0.56	14.96	0.05	M
125	-132.43	-122.25	15.97	0.73	0.94	0.45	13.90	0.10	B
126	-53.23	-122.08	15.06	1.53	1.87	0.98	10.94	0.02	

Table 4. - Continued

ID	XC(″)	YC(″)	V	$(B-V)$	$(V-I)$	$(V-R)$	K	σ_K	Membership
127	-28.55	-120.4	15.77	0.51	0.75	0.35	14.10	0.07	M
129	-146.48	-117.5	15.41	1.65	1.94	0.98	10.97	0.09	
133	-28.82	-115.48	17.46	1.09	1.33	0.68	14.70	0.08	
134	235.61	-114.4	16.20	1.17	1.62	0.84	12.83	0.03	
136	110.76	-111.38	15.33	0.57	0.79	0.35	13.75	0.03	M
137	187.43	-110.74	15.85	0.59	0.84	0.38	14.22	0.06	M
139	66.46	-109.96	12.82	0.39	0.56	0.25	12.01	0.06	M
140	181.41	-106.86	16.56	0.81	0.98	0.49	14.24	0.06	B
141	1.35	-106.84	16.89	0.83	1.19	0.59	14.51	0.01	B
142	-255.73	-101.81	17.15	1.06	1.31	0.70	14.38	0.08	
143	257.48	-101.78	13.62	1.48	1.73	0.92	9.95	0.04	
144	134.88	-100.1	16.66	0.89	1.21	0.64	14.30	0.09	
145	-20.24	-95.29	15.12	0.47	0.70	0.32	13.87	0.01	M
147	189.06	-92.97	17.29	0.74	1.15	0.32	15.03	0.07	
148	132.3	-90.45	16.38	1.05	1.26	0.69	13.91	0.04	
149	79.27	-89.47	15.30	0.46	0.65	0.33	13.97	0.00	M
151	-181.74	-88.81	15.58	0.57	0.70	0.32	14.12	0.06	M
152	142.35	-88.28	17.12	0.88	1.29	0.64	14.67	0.08	
153	133.43	-87.66	17.28	0.99	1.47	0.76	14.35	0.07	
155	-123.7	-84.8	15.94	0.57	0.71	0.34	14.59	0.09	M
157	-8.52	-83.33	15.62	0.47	0.75	0.37	14.20	0.00	M
158	85.81	-81.92	16.43	0.66	1.04	0.48	14.51	0.08	
159	-2.76	-80.96	16.48	0.61	0.98	0.53	14.40	0.02	M
160	-221.02	-80.31	13.20	1.50	1.58	0.82	9.64	0.05	
161	-238.01	-79.62	16.74	0.70	1.00	0.45	14.56	0.12	M
164	-36.03	-75.12	17.01	0.91	1.18	0.50	14.59	0.06	B
165	-147.02	-74.55	15.42	0.60	0.75	0.32	13.83	0.08	M
166	-131.22	-70.93	16.80	1.10	1.32	0.64	14.08	0.05	
169	-8.11	-69.28	16.24	0.61	0.78	0.35	14.68	0.05	M
171	196.41	-63.59	16.35	0.94	1.18	0.64	14.21	0.04	
173	-56.12	-61.03	15.79	1.38	1.66	0.89	12.47	0.01	
174	71.6	-60.78	13.19	1.19	1.46	0.76	10.26	0.02	
175	101.09	-60.41	13.29	1.15	0.73	0.35	12.02	0.02	
176	-237.59	-58.62	14.10	0.82	0.90	0.44	12.28	0.08	
178	-111.25	-56.81	17.56	1.06	1.37	0.70	14.73	0.09	
179	-86.84	-56.54	14.54	0.49	0.67	0.31	13.34	0.00	M
181	-166.49	-54.32	15.96	0.74	0.97	0.43	13.90	0.12	B
184	-213.84	-51.63	15.74	1.02	1.10	0.56	13.44	0.11	
186	-41.59	-50.68	17.57	0.88	1.24	0.57	14.98	0.02	M
187	40.86	-48.57	12.18	0.41	0.66	0.31	11.07	0.00	
189	-21.75	-47.61	14.98	1.56	1.81	0.94	10.91	0.01	
191	-92.45	-45.22	16.12	0.61	0.84	0.42	14.53	0.05	M
192	11.85	-44.58	15.31	0.45	0.69	0.32	13.97	0.07	M
193	113.34	-41.37	11.06	0.29	0.39	0.19	10.73	0.00	
194	-68.16	-40.97	15.69	0.53	0.70	0.30	14.31	0.01	M
195	-24.31	-39.96	15.31	0.55	0.73	0.35	13.94	0.06	M
198	-109.55	-37.72	14.73	0.47	0.63	0.27	13.57	0.01	M
199	-46.09	-36.87	17.13	0.91	1.30	0.66	14.57	0.03	
201	6.43	-36.15	15.89	0.68	0.98	0.48	14.04	0.03	B
202	72.5	-36.06	16.12	0.76	1.12	0.54	13.94	0.02	B
203	-191.01	-34.99	15.50	0.65	0.89	0.41	13.72	0.08	B
205	-24.85	-31.91	16.65	0.48	0.91	0.45	14.81	0.01	
206	-13.72	-31.24	16.60	0.71	0.92	0.44	14.87	0.01	M
207	-65.46	-30.06	16.00	0.56	0.69	0.29	14.64	0.02	M
209	36.02	-28.09	17.09	0.99	1.27	0.64	14.52	0.01	
210	14.25	-26.73	16.10	0.51	0.81	0.36	14.58	0.00	M
213	-41.57	-23.6	15.31	0.55	0.63	0.30	14.14	0.00	M
214	-84.78	-23.14	13.48	0.44	0.55	0.26	12.54	0.04	M
215	-35.67	-21.5	12.68	0.40	0.57	0.27	11.81	0.01	
219	167.56	-17.64	16.09	0.77	1.02	0.14	14.40	0.11	
220	76.8	-17.48	16.62	1.67	2.05	1.06	12.19	0.03	
223	-12.43	-13.81	14.96	0.84	1.03	0.54	12.96	0.02	
229	52.72	-11.13	14.68	0.75	0.99	0.48	12.89	0.00	
231	-52.12	-10.69	13.47	0.42	0.58	0.26	12.53	0.00	M
232	-47.01	-10.49	12.67	0.43	0.66	0.32	11.38	0.05	
236	186.88	-8.92	16.01	0.90	1.10	0.53	14.00	0.07	
237	-117.11	-6.78	16.78	1.12	1.39	0.70	13.84	0.08	
238	-24.94	-6.09	16.33	0.60	0.83	0.40	14.84	0.02	M
239	-64.41	-5.92	14.62	0.46	0.64	0.28	13.55	0.01	M
241	-54.06	-5.68	13.12	0.41	0.60	0.29	12.20	0.01	M
242	-85	-4.94	13.32	0.40	0.55	0.25	12.41	0.02	M

Table 4. - Continued

ID	XC(″)	YC(″)	V	$(B-V)$	$(V-I)$	$(V-R)$	K	σ_K	Membership
245	-114.97	-2.69	13.68	0.42	0.58	0.28	12.66	0.00	M
248	-105.7	-0.32	15.37	0.59	0.75	-0.20	13.97	0.03	
249	0	0	12.81	0.40	0.60	0.28	11.79	0.01	M
250	94.33	0.01	15.77	0.74	0.99	0.46	13.92	0.03	B
253	182.72	4.03	15.83	0.60	0.90	0.41	14.25	0.12	M
254	8.47	4.53	14.31	1.27	1.58	0.80	10.83	0.07	
255	36.96	5.52	14.70	0.41	0.64	0.31	13.72	0.02	M
256	49.5	6.93	13.32	0.45	0.70	0.33	12.14	0.01	M
258	4.38	8	15.94	0.60	0.78	-0.03	14.55	0.01	
259	71.7	8.66	15.77	0.65	0.87	0.38	14.03	0.01	
260	-78.13	9.98	14.65	1.48	1.76	0.90	10.80	0.02	
261	126.98	10.16	17.58	0.71	1.24	-0.06	15.09	0.05	
262	30.82	11.15	15.52	0.75	0.77	0.37	14.11	0.06	B
263	182.4	11.37	15.77	0.95	1.19	0.62	13.61	0.08	
264	54.18	11.5	15.28	-0.07	1.07	0.69	13.74	0.01	
266	85.46	12.46	17.19	0.62	1.20	-0.21	14.88	0.02	
268	-103.47	12.87	17.58	0.87	1.18	0.62	15.33	0.06	M
270	-71.01	16.24	17.17	0.98	1.09	0.56	14.71	0.02	B
271	-42.09	16.89	13.07	0.40	0.59	0.20	12.08	0.01	M
272	64.26	17.02	13.83	1.42	1.59	0.84	10.45	0.01	
274	-84.98	17.84	15.81	0.92	1.14	0.58	13.65	0.03	
275	-73.81	18.65	17.22	0.78	1.03	0.47	15.12	0.00	M
279	16.24	21.5	17.00	0.81	1.28	0.64	14.53	0.02	B
280	-64.35	22.23	14.77	0.44	0.63	0.30	13.68	0.04	M
282	150.56	23.05	17.31	0.81	1.18	0.59	15.01	0.17	M
284	-40.26	24.2	16.39	0.64	0.88	0.16	14.74	0.00	
285	-58.3	25.4	13.13	0.38	0.56	0.26	12.30	0.03	M
286	-63.13	27.44	17.27	0.76	1.16	0.56	15.09	0.01	M
287	50.75	28.11	15.57	1.36	1.55	0.79	12.33	0.03	
288	18.86	28.14	13.81	0.44	0.69	0.29	12.68	0.00	M
289	53.8	29.51	16.95	0.91	1.18	0.67	14.75	0.03	
290	56.4	30.93	16.52	0.97	1.21	0.62	14.16	0.02	
292	212.21	31.13	15.83	1.79	2.15	1.13	11.12	0.29	
293	-91.22	32.54	16.80	0.76	0.92	0.46	14.78	0.02	M
295	-8.5	34.4	14.12	0.41	0.61	0.28	13.16	0.01	M
296	38	35.02	15.21	1.51	1.76	0.91	11.43	0.04	
297	-57.07	36.04	15.68	0.50	0.68	0.31	14.54	0.00	M
298	237.01	36.7	16.59	1.57	1.99	1.02	12.49	0.18	
300	-127.44	38.65	15.26	0.84	1.02	0.54	13.16	0.10	
302	-42.53	40.16	14.33	0.72	0.56	0.23	13.39	0.01	
303	193.69	40.87	15.73	1.41	1.90	0.98	11.71	0.18	
304	-94.04	41.17	16.69	0.71	0.97	0.41	14.86	0.00	M
305	148.8	43.66	17.53	0.82	1.24	0.65	14.80	0.16	M
306	-41.21	43.84	13.50	0.43	0.60	0.22	12.40	0.07	M
307	23.5	45.54	16.67	0.73	1.04	0.45	14.54	0.00	M
310	-48.69	51.34	17.47	0.86	1.31	0.69	14.91	0.03	
311	-177.63	54.32	15.94	0.54	0.67	0.32	14.55	0.09	M
312	237.8	58.88	15.08	0.76	0.79	0.41	13.80	0.17	
313	-15.64	61.33	16.03	0.76	1.10	0.51	13.95	0.02	B
314	-64.38	61.36	15.96	0.56	0.74	0.32	14.53	0.06	M
315	29.25	61.55	16.94	0.80	1.24	0.57	14.56	0.02	B
316	-0.98	62.03	17.02	1.07	1.34	0.67	14.30	0.03	
317	-115.57	63.78	15.79	0.54	0.67	0.31	14.38	0.09	M
318	40.71	66.98	14.74	1.37	1.63	0.85	11.25	0.01	
319	-100.7	68.79	16.58	0.62	0.91	0.42	14.77	0.05	M
321	-13.13	75.23	16.06	0.59	0.78	0.38	14.67	0.02	M
322	161.26	75.59	17.20	0.85	1.12	0.51	14.81	0.11	M
323	-50.59	76	13.29	0.68	0.87	0.45	11.63	0.01	
324	10.47	76.03	16.75	0.86	1.11	0.52	14.55	0.03	B
325	-100.44	76.4	16.94	0.69	0.98	0.49	14.94	0.05	M
326	-220.14	76.8	15.84	0.87	1.01	0.53	13.65	0.07	
327	-96.1	77.34	16.05	1.15	1.39	0.77	13.23	0.02	
329	-59.76	77.98	16.85	0.61	1.03	0.50	14.95	0.05	
330	15.32	78.83	16.71	0.70	0.97	0.41	14.92	0.07	M
331	-72.74	79.39	16.19	1.05	1.32	0.68	13.56	0.00	
333	54.61	83.44	14.81	2.10	1.48	0.75	11.80	0.01	
334	135.85	84.5	17.53	0.87	1.32	0.62	14.63	0.22	M
335	17.52	86.37	16.04	0.56	0.83	0.37	14.56	0.03	M
336	177.18	87.2	17.51	0.87	1.18	0.60	15.10	0.12	M
337	-87.75	88.86	15.02	0.80	0.99	0.50	13.11	0.05	
338	-83.48	93.58	16.43	0.88	1.16	0.56	14.05	0.03	

Table 4. - Continued

ID	XC($''$)	YC($''$)	V	$(B-V)$	$(V-I)$	$(V-R)$	K	σ_K	Membership
339	121.11	95.02	16.89	0.11	1.75	1.18	13.96	0.27	
341	-182.93	95.92	16.28	1.02	1.19	0.59	13.89	0.09	
342	209.38	96.87	15.66	0.94	1.21	0.62	13.11	0.19	
344	-52.56	97.79	16.98	0.78	1.04	0.53	14.84	0.02	M
345	48.61	99.7	15.44	0.51	0.82	0.38	14.00	0.01	M
346	158.27	99.78	17.13	1.46	1.84	0.95	13.08	0.15	
347	-94.63	100.84	16.88	0.76	0.95	0.41	14.97	0.01	M
348	44.25	101.9	16.97	0.71	1.03	0.49	15.11	0.05	M
349	106.57	102.01	16.25	1.53	2.00	1.04	11.90	0.13	
350	99.4	103.45	15.19	0.46	0.69	0.33	13.87	0.18	M
351	-72.9	104.15	17.47	0.93	1.18	0.57	15.13	0.03	M
352	-145.16	104.74	17.06	1.18	1.27	0.62	14.49	0.10	
353	-90.73	107.34	16.91	1.19	1.40	0.74	14.10	0.10	
354	5.37	107.68	13.70	1.30	0.96	0.48	12.00	0.04	
355	-135.49	107.81	17.38	1.05	1.21	0.65	14.83	0.09	
356	-203.64	110.13	16.80	0.88	1.12	0.49	14.49	0.12	B
357	56.01	111.98	16.96	0.97	1.24	0.64	14.55	0.03	
358	165.68	115.11	14.98	0.43	0.67	0.33	13.63	0.16	M
359	43.59	116.49	16.67	0.64	0.95	0.46	14.79	0.03	M
361	-114.88	117.62	16.99	0.92	1.22	0.62	14.70	0.10	
362	173.24	118.07	16.00	0.38	1.08	0.61	13.91	0.17	
363	-180.96	118.6	16.69	0.69	0.87	0.22	15.11	0.09	
364	-37.33	120.28	17.30	0.94	1.24	0.59	14.90	0.01	B
365	90.09	120.86	16.15	0.56	0.76	0.38	14.41	0.11	M
366	110.48	121.29	14.92	0.68	1.00	0.48	12.90	0.25	
367	-226.82	121.57	16.45	0.70	0.95	0.44	14.49	0.08	M
369	-13.93	123.92	17.28	0.81	1.16	0.58	14.95	0.02	M
371	100.24	129.08	15.38	0.77	1.20	0.31	13.02	0.18	
373	81.3	133.26	16.05	0.74	0.98	0.52	14.23	0.19	B
375	18.18	134.9	15.25	0.46	0.73	0.33	13.95	0.10	M
376	-15.6	135.3	17.02	0.97	1.25	0.62	14.52	0.07	
377	-1.39	135.82	17.06	0.89	1.18	0.62	14.49	0.13	B
378	112.14	136.82	13.74	0.38	0.60	0.27	12.69	0.09	M
379	-206.82	137.02	15.84	1.50	1.79	0.90	11.99	0.05	
382	-239.63	140.23	17.09	0.26	1.28	0.79	14.68	0.10	
385	-132.74	142.48	13.17	0.51	0.60	0.24	12.05	0.04	M
386	220.24	145.91	15.20	0.79	0.98	0.53	13.49	0.20	
387	260.57	146.88	16.89	1.46	2.00	1.00	12.47	0.17	
388	33.87	148.38	15.83	0.48	0.76	0.36	14.48	0.12	M
389	-144.57	148.62	13.51	0.47	0.65	0.30	12.34	0.09	M
391	79.86	149.99	16.49	1.27	1.92	0.96	12.48	0.14	
394	-235.96	152.34	14.26	0.58	0.78	0.35	12.73	0.08	M
395	-241.87	154.62	14.43	0.76	0.87	0.44	12.80	0.07	
396	-182.94	155.62	14.52	0.51	0.71	0.33	13.27	0.05	M
397	-66.01	156.84	16.09	1.53	1.92	1.00	12.00	0.08	
398	167.18	158.57	17.16	0.92	1.14	0.61	14.99	0.21	B
400	90	163.5	16.89	1.05	1.24	0.63	14.36	0.19	
401	151.15	164.84	16.42	1.38	1.66	0.89	12.82	0.16	
402	-111.27	167.43	15.02	0.59	0.90	0.54	13.28	0.08	
403	76.84	167.76	15.74	0.48	0.77	0.38	14.40	0.22	M
404	226.64	169.63	16.94	0.67	0.98	0.43	15.01	0.13	
405	-89.02	170.89	16.53	0.63	0.87	0.01	14.86	0.09	
406	-93.67	171.35	16.14	0.74	1.00	0.48	14.08	0.12	B
407	-82.39	172.54	16.54	0.77	1.13	0.58	14.43	0.11	B
409	-27.22	172.9	16.57	0.56	0.87	0.42	14.73	0.12	
411	-56.71	175.31	17.23	0.88	1.26	0.60	14.61	0.12	B
414	90.32	178.44	16.52	0.98	1.19	0.65	14.09	0.13	
415	-3.23	178.5	15.46	0.74	1.03	0.47	13.44	0.09	
416	240.2	179.27	16.90	1.61	2.06	1.10	12.43	0.15	
417	258.89	180.37	16.64	1.72	2.06	1.09	12.14	0.09	
418	-209.17	185.95	17.64	0.88	1.22	0.55	15.04	0.06	M
419	34.37	186.49	15.42	0.79	1.05	0.54	13.40	0.11	
420	-213.66	187.83	16.25	0.66	0.95	-0.12	14.38	0.08	
422	-233.55	189.82	14.65	1.26	1.42	0.71	11.68	0.07	
423	72.78	191.11	16.42	0.80	1.07	0.53	14.44	0.15	B
424	194.46	193.49	15.64	0.31	1.04	0.61	13.83	0.16	
425	189.45	194.08	15.11	0.68	0.85	0.44	13.61	0.24	
426	240.51	195.23	16.68	0.97	1.38	0.78	14.17	0.10	
427	-103.34	195.31	13.51	1.46	1.65	0.88	9.91	0.07	
428	75.93	197.47	16.42	1.63	1.99	1.04	12.09	0.08	
429	-118.86	197.87	15.27	0.77	1.01	0.51	13.37	0.09	

Table 4. - Continued

ID	XC(″)	YC(″)	V	$(B-V)$	$(V-I)$	$(V-R)$	K	σ_K	Membership
430	-182.8	198.02	15.79	0.64	0.94	0.45	14.05	0.08	
431	-53.21	202.25	16.51	0.78	1.21	0.67	14.14	0.08	
432	-165.92	206.71	17.10	1.53	1.97	1.01	12.97	0.08	
434	207.42	209.78	15.83	0.80	1.20	0.62	13.66	0.16	
435	-74.39	210.32	13.58	0.77	0.74	0.39	12.42	0.11	
436	-239.58	213.92	15.78	0.58	0.89	0.38	14.13	0.04	M
438	-174.18	216.89	16.53	0.69	0.95	0.41	14.77	0.15	M
442	-59.3	226.82	16.54	0.64	0.99	0.49	14.58	0.12	M
443	73.04	228.53	15.24	0.64	0.96	0.51	13.53	0.12	
444	136.23	229.9	13.53	0.40	0.57	0.28	12.78	0.16	M
447	-57.06	236.13	16.01	0.52	0.65	0.13	14.34	0.07	
450	165.76	238.31	17.57	0.70	1.09	0.55	15.44	0.17	
451	-171.98	240.26	15.21	0.78	1.01	0.24	13.35	0.06	

Cluster membership will be tested only for these stars in Section III-(c).

III. ANALYSIS

(a) Distance and Reddening

Color-magnitude diagrams and color-color diagrams of the cluster are presented in Fig. 4 and Fig. 5, respectively. In (a), (b), and (c) of Fig. 4, large dots represent the stars with errors in V-magnitude less than 0.1 mag and with errors in color less than 0.05, and the filled squares denote Cepheid variables. In Fig. 4(d), only stars with B, V, R, I, and K magnitudes are presented. The color-magnitude diagram of NGC 7790 shows a rather broad sequence with severe field contamination. The stars in the redder part of the color-magnitude diagrams, with (B-V) > 1.5, are easily recognized to be field stars, but near the main-sequence it is very hard to distinguish cluster members from field stars. However, overall the main-sequence and turn-off are relatively well understood.

The distance modulus and the reddening were obtained using the empirical ZAMS of Sung & Bessell(1999) which is mainly fitted to the (V, V-I) CMD where the main-sequence is the deepest and the field stars are relatively well isolated compared to the other color magnitude diagrams. The empirical ZAMS line was determined from photometric data for the young open cluster NGC 6231(Sung et al. 1998a), NGC 6611(Sung et al. 1998b), and the intermediate-aged open cluster M35(Sung & Bessell 1999). The best fit to the (V,V-I) CMD is shown in Fig. 6(b). For the ratio of total to selective extinction, we have adopted $R = A_V/E(B-V) = 3.06$ (Olson 1975; Walker 1987) as in RBFT, although $R = 3.1$(Mateo & Madore 1988), 3.24(Gieren & Fouque 1993), have been used more recently. We adopted a general interstellar color excesses ratio(He et al. 1995):

$$E(V-R)/E(B-V) = 0.61$$

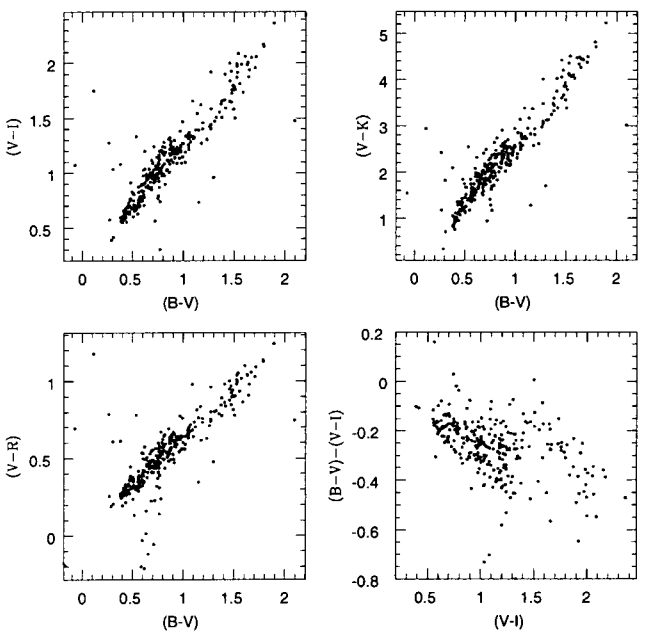

Fig. 5.— Color-Color Diagram of NGC 7790.

$$E(V-I)/E(B-V) = 1.35$$
$$E(V-K)/E(B-V) = 2.76$$

The measured distance modulus and the reddening are $(m-M)_o = 12.45 \pm 0.10$, and $E(B-V) = 0.54 \pm 0.05$. The distance modulus of this study is midway between the values $(m-M)_o = 12.65 \pm 0.15$ of RBFT and $(m-M)_o = 12.33 \pm 0.15$ of Mateo & Madore (1988), while the reddening is consistent with the values $E(B-V) = 0.54 \pm 0.04$ of RBFT and $E(B-V) = 0.56$ of Mateo & Madore (1988).

NGC 7790 contains three classical Cepheid variables which are thought to be members of the cluster. From their periods and apparent magnitudes, the distance

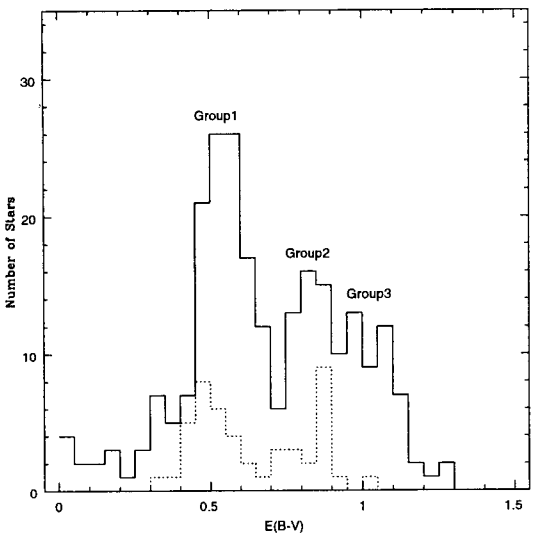

Fig. 7.— Color excess E(B-V) distribution. The solid line is the distribution of all stars measured in B,V,R,I,K. There are three groups (1, 2, & 3). Group 1 denotes cluster members. The dotted line is the distribution of Group 2 after applying a magnitude correction of 0.75 mag for equal magnitude binaries.

moduli can be calculated. The period and mean V magnitude of CF Cas are known to be 4.88^d and 11.16 mag(Matthews et al. 1995) and those of CE Cas a and CE Cas b are 5.14^d, 10.90 mag, and 4.48^d, 11.04 mag(Opal et al. 1988), respectively. The known period-luminosity relation for Cepheids (Larney & Stobie 1994) predicts the absolute magnitude as follows:

$$M_V = -4.071(\pm 0.056) - 2.874(\pm 0.072)(logP - 1)$$

If we apply this relation to the three Cepheids, the absolute V magnitude M_V is -3.18 for CF Cas, -3.24 for CE Cas a, and -3.06 for CE Cas b. Adopting E(B-V)=0.54, the distance modulus is $(m - M)_o$ = 12.69, 12.49, and 12.45 for CF Cas, CE Cas a, and CE Cas b, respectively. The case of CF Cas is slightly different , but the cases of CE Cas a and CE Cas b are consistent with the CMD results.

(b) Age Determination

The age of the cluster was estimated by fitting the theoretical isochrone of Bertelli et al. (1994) to the observed CMD. However, when theoretical isochrones are used for age determination, the metallicity of the cluster is needed.

Based on Washington photometry of CF Cas, Harris(1981) found the star's metallicity to be $[A/H] \sim -1$. Panagia & Tosi(1981) found that NGC 7790 is slightly metal deficient, with [A/H]$\simeq -0.3$(assuming a helium abundance of Y=0.28, this corresponds to a metallicity of Z=0.01) but this metallicity for NGC 7790 should be changed to [Fe/H]=-0.13 if the recent mean radial abundance gradient of Piatti et al. (1995) and a galactic distance of R_{GC} =10.4kpc for NGC 7790 which is based on a solar distance of 8.5kpc, are applied.

If the three Cepheids are indeed cluster members - a fact which is generally accepted, we can constrain the metallicity range of the cluster. According to evolutionary theory, these Cepheids in NGC 7790 are supposed to be in the second passage to the red giant phase. Therefore we have to assume the cluster's metallicity to be [Fe/H]=-0.32 (z = 0.008) in order to place the Cepheids at the blue loop of a proper isochrone. The best fits to the CMD are shown in Fig. 6. Considering the location of the three Cepheids in the CMDs, we can constrain the age of the cluster to $\log(age) = 8.1 \pm 0.1$. This agrees with RBFT's age of $(1.0 \pm 0.2) \times 10^8 yr$ which was used in overshooting models(Bertelli et al. 1986).

(c) Membership

We have tried a photometric method to select the member stars of NGC 7790 using all four color indices. Generally, the best way to check membership is to obtain the proper motions or radial velocities of stars but NGC 7790 is too distant to determine these for individual stars. However, four color indices make it possible to use a photometric method to select the members.

The membership search was done only for stars having all B, V, R, I, and K magnitudes. First, we adopted the derived distance modulus, $(m - M)_o$=12.45, which was obtained by main sequence fitting in Section III (a). Then intrinsic colors for a star were calculated from the isochrone using the observed V magnitude. Using different color excesses($E(B-V)$) from 0 to 1.5, the expected colors for each star were calculated. The calculated color for each star was compared to the observed one. We define χ^2 as the following:

$$\begin{aligned}\chi^2 = & [(B-V)_{obs} - (B-V)_{cal}]^2 \\ & + [(V-I)_{obs} - (V-I)_{cal}]^2 \\ & + [(V-R)_{obs} - (V-R)_{cal}]^2 \\ & + [(V-K)_{obs} - (V-K)_{cal}]^2\end{aligned}$$

The color excess $E(B-V)$ of each star was determined by the lowest χ^2 value. The distribution of color excess $E(B-V)$ is shown in Fig. 7. The Fig. 7 shows the main peak near $E(B-V) \sim 0.5$ and two relatively large color-excess peaks at $E(B-V) \sim 0.8$ and 1.1. The stars around the main peak at $E(B-V) \sim 0.5$ are regarded as cluster members and the color excess values of these stars are reasonable enough to be counted as members. Their mean $E(B-V)$ is 0.547 with a standard deviation of 0.075, which agrees with $E(B-V)$ of 0.54±0.05 previously determined by ZAMS fitting in Section III.

The stars near the peak around $E(B-V) \sim 0.8$ are now further investigated. There is a probability that some of stars around this peak are binary members of

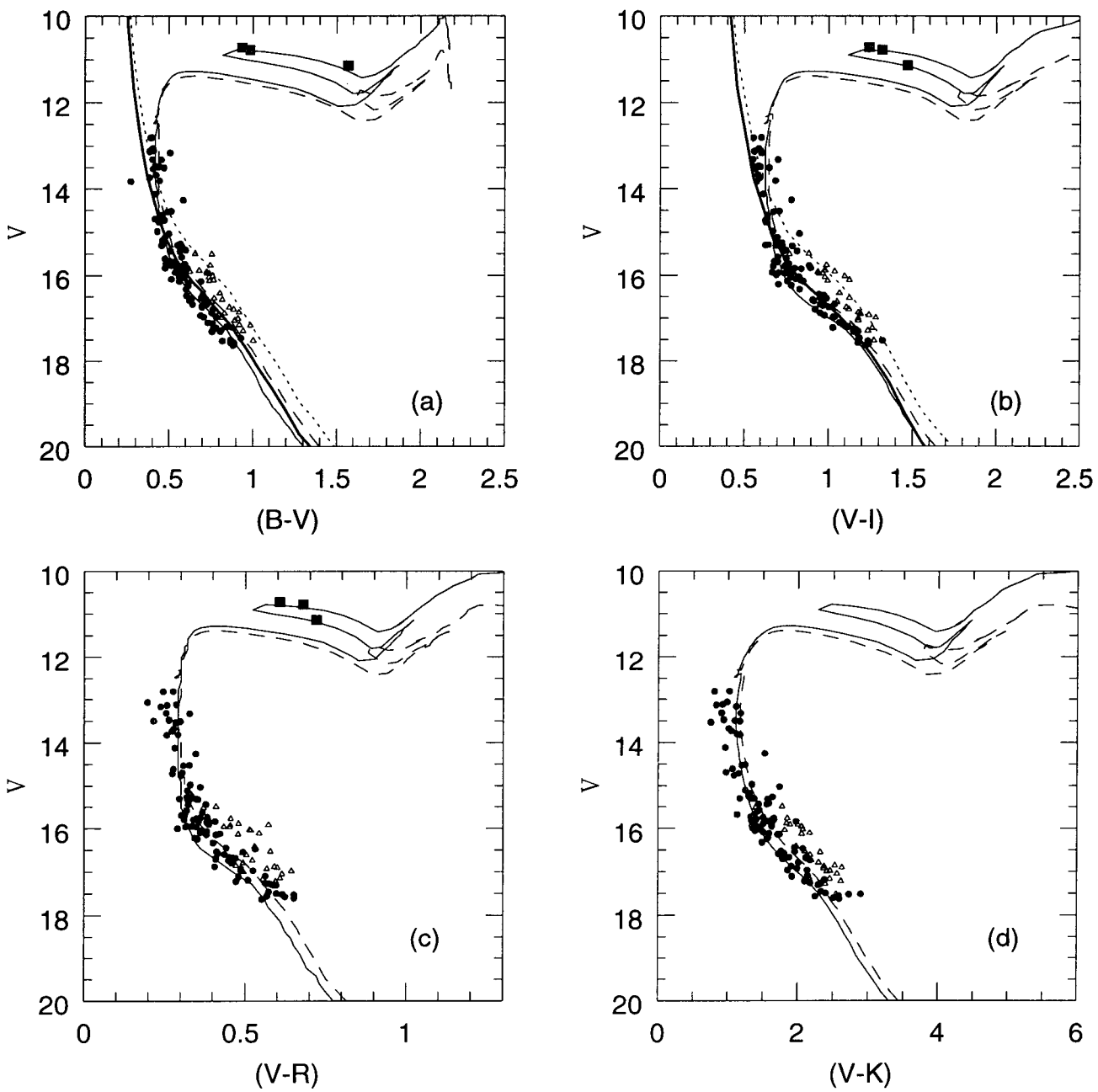

Fig. 8.— CMDs with only cluster members. The filled circles represent single stars and the open triangles are binary members. The thick solid line is the ZAMS line, the thin solid line is the theoretical isochrone of [Fe/H]=-0.32, the dashed line is the isochrone of [Fe/H]=0.07(Bertelli et al. 1994), and the dotted line indicates the equal mass binary sequence. The filled squares represent Cepheids.

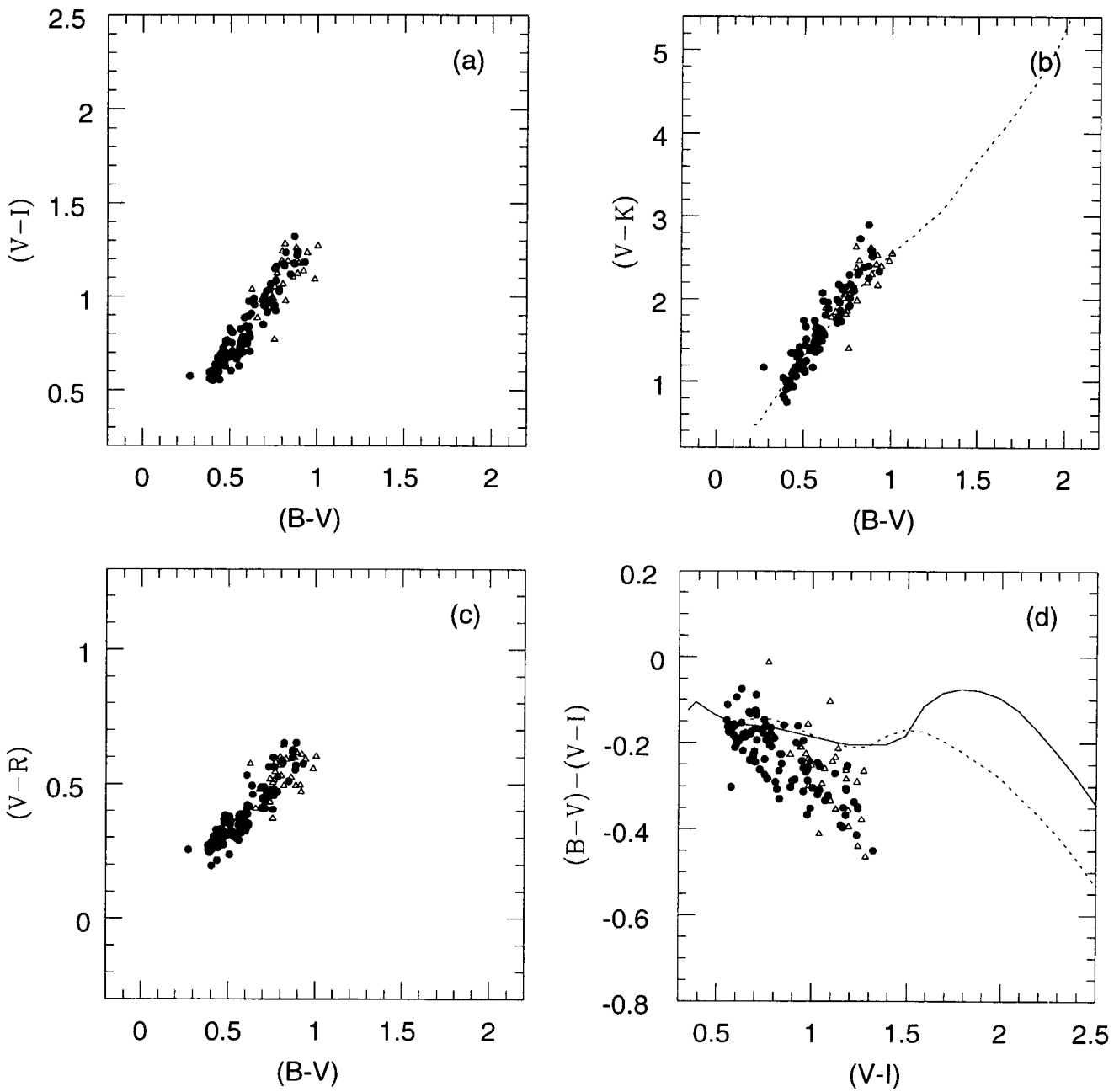

Fig. 9.— CMDs with only cluster members. The filled circles represent single stars and triangles are binary members. In (b), the dotted line is the mean line of the field dwarfs (Johnson 1968). In (d), the solid line is the giant mean line and the dotted line is the MS mean line.

the cluster. So we assumed all the stars around this peak are binary members which have equal masses. Then their V magnitudes are brighter by 0.75 mag than the single star of the same mass. Thus the magnitudes of these stars were corrected by 0.75 mag, and then their $E(B-V)$ was recalculated. The corrected distribution of these stars is shown in Fig. 7 with a dotted line indicating two subgroups. One peaks near $E(B-V) \sim 0.5$, indicating probable binary members of the cluster, and the other peaks around $E(B-V) \sim 0.8$, implying probable field stars. These binary candidates are indicated by a "B" in the last column of Table 4. The peak around $E(B-V) \sim 0.8$ and 1.1 may not have any astronomical significance. Since the distance modulus of the cluster was adopted for all stars in the field, the measured color excesses of non-member stars are not their real color excesses.

We have compared our membership test results to those of RBFT. There are 131 stars in common with the RBFT data. They also checked the membership using (V,B-V), (V,V-I) CMDs and classified the stars into three groups: A, B, and non-members. Stars of 'class A' were determined to be members in both (V,B-V) and (V,V-I) CMDs and stars of 'class B' were determined to be members in one of the two CMDs. Among the stars in common, 72 stars are 'class A', 17 stars are 'class B', and 42 stars are non-members. About seventy percent of stars were found to be members by RBFT.

Among the 131 common stars, 71 stars were determined to be member stars in our study. That means only fifty four percent of the stars are found to be members by our method. We have found that among the 'class A' stars of RBFT 54 stars are determined to be cluster members, 3 stars as binaries, and 15 stars are rejected as non-members in our study. For 'class B', 7 stars are found to be single member stars, 7 stars are binary members, and 3 stars are non-member stars. Since our method of using four color indices is more rigorous than RBFT's, it is reasonable that fewer stars are found to be members in our study. However, the fact that three out of 42 stars, which were found to be non-members by RBFT, have been found to be members in this study, makes the uncertainty in membership by this method greater than about 7%.

Fig. 8 shows color magnitude diagrams for members of the cluster only. The thick solid lines represent the ZAMS and the thin solid lines and the dashed lines are theoretical isochrones with [Fe/H]= -0.32 and [Fe/H]= 0.07, and the dotted line indicates the equal mass binary sequence. The filled circles are the single members, and the triangles are binary members. The CMD shows that binary stars which have been identified by this method coincide well with the binary sequence. Fig. 9 shows color-color diagrams for the members. In the CCD of Fig. 9(b), the main sequence stars of the cluster are consistent with the dotted line of the mean line of field dwarfs(Johnson 1966). Comparing with Fig. 5, the smaller color ranges of Fig. 9 are due to the cutoff in V magnitude at about 18 mag, which limits the (B-V) color of the main sequence to bluer colors ($\lesssim$1.0), as well as due to the removal of the field stars.

However, stars redder than the main sequence line and brighter than the main sequence cutoff are removed, mainly due to non-membership. In Fig. 9(d), the single members are consistent with the mean lines of the giant and main sequences.

IV. CONCLUSION

Although the observations involving BVRI CCD photometry and NIR K photometry of open cluster NGC 7790 were performed on non-photometric days, the derived reddening and distance modulus are quite reasonable compared to the results of previous studies. The K-band observations were not so helpful for the determination of $E(B-V)$ and the distance modulus because of their large errors but were useful for determination of membership by providing another color term and for presenting information on the K magnitudes of the cluster.

Using ZAMS fitting, we derived a reddening of $E(B-V) = 0.54 \pm 0.04$ and a distance modulus of $(m-M)_o = 12.45 \pm 0.10$. The age, $\log(age) = 8.1 \pm 0.1$ of the cluster was estimated using a theoretical isochrone(Bertelli et al. 1994), adopting [Fe/H]=-0.32. Although this metallicity places the Cepheids of NGC 7790 at the blue loop of the corresponding isochrone, the metallicity of NGC 7790 is more likely to lie between $-0.32 < [Fe/H] < 0.07$ on the basis of the isochrone along the main sequence, which is seen in Fig. 8. However, if we adopt a metallicity of [Fe/H] =0.07, the Cepheids of the cluster are located in the bluer region of other corresponding isochrones of the same age. Therefore, the metallicity of this cluster is still uncertain and needs further investigation.

The color excesses for each star were determined by adopting the derived distance modulus, and from the distribution of the resulting color excesses for stars, we distinguished not only single members but also binary members. We have checked cluster membership for 297 stars which all have B, V, R, I, and K magnitudes and these are listed in Table 4. Among them, 101 stars were found to be single members, while 30 stars were found to be binary member stars. About seventy percent of them were determined to be members by RBFT.

Further study on the luminosity and mass functions of NGC 7790 will be discussed in a subsequent paper(Lee & Lee 1999).

This work was supported in part by the Basic Science Research Institute Program, Ministry of Education, BSRI-98-5411.

REFERENCES

Alibert, Y., Baraffe, I., Hauschildt, P., & Allard, F. 1999,

A&A, 344, 551

Bertelli, G., Bressan, A., Chiosi, C., & Angerer, K., 1986, A&AS, 66, 191

Bertelli, G., Bressan, A., Chiosi, C., Fagotto, F., & Nasi, E. 1994, A&AS, 106, 205

Casali, M., & Hawarden, T., 1992, The JCMT-UKIRT newsletter, 4, 33

Christian, C. A., Adams, N., Barnes, J. V., Butcher, H., Hays, D. S., Mould, J. R., & Siegel, M. 1985, PASP, 97, 363

Gieren, W. P., & Fouque, P. 1993, AJ, 106, 734

He, L., Whittet, D. C. B., Kilkenny, D., & Spencer Jones, J. H., 1995, ApJS, 101, 335

Janes, K. A. 1979, ApJS, 49, 425

Janes, K. A., & Adler, D. 1982, ApJS, 49, 425

Janes, K. A., & Phelps R. L., 1994, AJ, 108, 1773

Johnson, H. L. 1968, in Nebulae and Interstellar Matter, ed. B. M. Middlehurst & L. H. Aller (Chicago & London:University of Chicago Press), 194

Johnson, H. L. 1966, ARA&A, 4, 193

Kraft, R. P. 1958, ApJ, 128, 161

Kraft, R. P. 1961, ApJ, 134, 616

Landolt, A. U. 1983, AJ, 88, 439

Larney, C. D., & Stobie, R. S. 1994, MNRAS, 266, 441

Lee, S. -G., Carney, B. W., & Oh, S. J. 1998, private communication

Lee, S. -G., Carney, B. W., & Probst, R. 1997, JKAS, 30, 1

Lee, J. -D., & Lee, S. -G. 1999, in preparation

Lyngå, G. 1987, Catalog of Open Cluster Data, 5th ed.

Mateo, M., & Madore, B. 1988, PASP, 100, 1222

Matthew, J. M., Gieren, W. P., Mermilliod, J. C., & Welch, D. L. 1995, AJ, 110, 2280

Mermilliod, J. C. 1981, A&A, 97,235

Opal, C. B., Krist, J. E., & BarnesIII, T. G., 1988, AJ, 96, 1677

Panagia, N., & Tosi, M. 1981, A&A, 97, 235

Piatti, A. E., Claria, J. J., & Abadi, M. G. 1996, AJ, 110, 281

Pedreros, M. H., Madore, B. F., & Freedman, W. L. 1984, ApJ, 286, 563 (PMF)

Romeo, G., Bonifazi, A., Fusi Pecci, F., & Tosi, M. 1989, MNRAS, 240, 459 (RBFT)

Sandage, A. R. 1958, ApJ, 128, 150

Sandage, A. R., & Tammann, G. A. 1969, ApJ, 151, 683

Sekiguchi, M., & Fukugita, M. 1998, The Observatory, 119, 73

Schmidt, E. G. 1981, AJ, 86, 242

Stetson, P. B. 1987, PASP, 99, 191

Stetson, P. B. 1990, PASP, 102, 932

Sung, H., Bessell, M. S., & Lee, S.-W. 1998a, AJ, 115, 734

Sung, H., Lee S.-W., & Bessell, M. S. 1998b, in preparation

Sung, H., & Bessell, M. S. 1999, MNRAS, 306, 361

Tanvir, N. R. 1997, in Extragalactic Distance Scale, Proceedings of the STScI May Symposium, ed. M. Livio, M. Donahue, & N. Panagia, 91

Walker, A. R. 1987, MNRAS, 229, 31